ELSEVIER

Microporous and Mesoporous Materials 55 (2002) 203–216

MICROPOROUS AND MESOPOROUS MATERIALS

www.elsevier.com/locate/micromeso

Framework cobalt and manganese in MeAPO-31 (Me = Co, Mn) molecular sieves

Nataša Novak Tušar [a,*], Gregor Mali [a], Iztok Arčon [b,c], Venčeslav Kaučič [a,d], Afshin Ghanbari-Siahkali [e], John Dwyer [e]

[a] *National Institute of Chemistry, Hajdrihova 19, 1000 Ljubljana, Slovenia*
[b] *School of Environmental Sciences, Vipavska 13, 5001 Nova Gorica, Slovenia*
[c] *Institute Jožef Stefan, Jamova 39, 1000 Ljubljana, Slovenia*
[d] *Biotehnical Faculty, University of Ljubljana, Jamnikarjeva 101, 1000 Ljubljana, Slovenia*
[e] *Centre for Microporous Materials, UMIST, P.O. Box 88, Manchester M60 1QD, UK*

Received 3 September 2001; received in revised form 14 December 2001; accepted 18 March 2002

Dedicated to Professor Sergey Petrovich Zhdanov on the occasion of his 90th birthday

Abstract

Pure phases of CoAPO-31 and MnAPO-31 were synthesized hydrothermally using di-*n*-propylamine as a structure-directing agent. The incorporation of manganese(II) and cobalt(II) into framework aluminum sites of $AlPO_4$-31 was suggested from elemental, thermogravimetric and X-ray powder diffraction analysis. Isomorphous aluminum substitution with cobalt(II) was confirmed from static ^{31}P NMR spectra. UV–VIS and XANES spectra revealed a partial oxidation of framework cobalt(II) and manganese(II) into cobalt(III) and manganese(III) in the calcined MeAPO-31 and thus the presence of redox centers in the products. The generation of acid sites (Brønsted and Lewis) in MeAPO-31 was supported by IR measurements of pyridine and by ammonium adsorption/desorption. The strength of the acid sites in the catalysts studied decreased in the following order: MnAPO-31 > CoAPO-31 > $AlPO_4$-31.

Keywords: Hydrothermal synthesis; Metal substituted aluminophosphates; MeAPO-31; Framework cobalt and manganese; Catalytically active centers

1. Introduction

$AlPO_4$-31 with an ATO framework topology is a medium-pore aluminophosphate molecular sieve with a one-dimensional pore system of 0.53 nm pore diameter [1]. Powder X-ray diffraction measurements on calcined $AlPO_4$-31 revealed a rhombohedral symmetry (hexagonal setting, $a = b = 20.827(1)$ Å, $c = 5.003(1)$ Å, and space group R-3) [1]. The rhombohedral symmetry was also determined for the as-synthesized SAPO-31 [2]. Recently [3], a powder X-ray diffraction pattern, without structure refinement, of as-synthesized $AlPO_4$-31 indicated a lower, triclinic symmetry ($a = 12.23(3), b = 12.27(3), c = 12.54(3), \alpha = 112.7(2)°, \beta = 113.9(2)°, \gamma = 112.5(2)°$) [3].

* Corresponding author. Tel.: +386-1-47-60-371; fax: +386-1-47-60-300.

1387-1811/02/$ - see front matter
PII: S1387-1811(02)00404-3

After the incorporation of a small amount of metal (Zn, Mg) into the $AlPO_4$-31 framework, the symmetry changed to rhombohedral [3]. This suggests that substitution of framework elements by metals may have occurred.

Isomorphous substitution of framework phosphorus in SAPO-31 by silicon was first proved using single-crystal diffraction on the as-synthesized sample [2]. Phosphorus substitution was later confirmed using several characterization methods [4–7] and was supported by several catalytic reactions such as hydrocarbon transformations [8–12]. Suggestions for the incorporation of other metals into the $AlPO_4$-31 framework can be found in three publications for TAPO-31 [13], ZnAPO-31 [3] and MgAPO-31 [3,14], and catalytic applications are reported for TAPO-31 [15], VAPO-31 [16], MnAPO-31 [8,17], NiAPO-31 [17], ZnAPO-31 [17] and FeAPO-31 [18]. However, no literature reports could be found providing direct evidence for the isomorphous substitution of framework aluminum in $AlPO_4$-31 by cobalt or manganese.

CoAPO-*n* and MnAPO-*n* catalysts (*n* denotes a specific structure type) have recently been shown to oxidize linear alkanes using molecular oxygen as reagents, rather than more expensive oxidants such as organic hydroperoxides [19]. The local coordination of manganese and cobalt ions in MeAPO-*n* molecular sieve frameworks is related to the structural features of the $AlPO_4$-*n* system, the amount of metal loading and the preparation procedure [20]. Different characterization techniques were used to obtain information about the isomorphous substitution of framework atoms in MeAPO-*n* by cobalt and manganese [20]. It was found that only part of the framework cobalt(II) and manganese(II) ions can be oxidized to cobalt(III) and manganese(III) ions and, consequently, can be catalytically active. Extra-lattice manganese(II) ions have also been detected in most studies. Recently, ab initio quantum chemical techniques have been applied for investigating the structural and bonding properties of microporous cobalt-substituted aluminophosphates [21]. The results of these calculations are in agreement with experimental structural data and suggest a molecular-ionic character for the bonding in $AlPO_4$-*n* materials comprising Al^{3+} and PO_4^{3-} ions. Moreover, a coordination number lower than 4 for the framework cobalt(III) ions in calcined CoAPO-*n*, suggested from X-ray absorption fine structure (EXAFS) studies [22], is explained by these calculations.

In the present study we prepared pure and highly crystalline $AlPO_4$-31 and MeAPO-31 (Co, Mn) products, and used several spectroscopic techniques to demonstrate the substitution of metal ions into MeAPO-31 and the generation of sites having potential catalytic activity.

2. Experimental

2.1. Synthesis

$AlPO_4$-31 and MeAPO-31 were synthesized hydrothermally, in the presence of di-*n*-propylamine (Pr_2NH, Merck, 99%) as a template, in stainless steel teflon-lined autoclaves under static conditions. The aluminum and phosphorus sources were pseudo-boehmite (PURAL SBI, Condea, 75.3% Al_2O_3) and phosphoric acid (H_3PO_4, Merck, 85%), respectively. Metal acetate hydrates ($Mn(CH_3COO)_2 \cdot 4H_2O$ Merck, >99% and $Co(CH_3COO)_2 \cdot 4H_2O$, Fluka, >99%) were used as metal sources.

The synthesis procedures, chosen according to the literature reports on SAPO-31 [2,4–7] and MeAPO-31 [8,14–16], were systematically studied and optimized. Final molar compositions of the reaction mixtures and the synthesis conditions for the preparation of pure $AlPO_4$-31 and MeAPO-31 (Me = Co, Mn) phases are given in Table 1. $AlPO_4$-31 was prepared from an aqueous slurry of pseudo-boehmite. Orthophosphoric acid and di-*n*-propylamine were added successively to the stirred slurry. The reaction mixture was then thoroughly blended for 10 min using a disperser.

The synthesis of MeAPO-31 (Me = Co, Mn) started with the preparation of three solutions/dispersions. The water content of the total gel in precent is indicated in each case. Metal acetate was dissolved in 20%, pseudo-boehmite dispersed in 50% and orthophosphoric acid diluted with 30% of the required quantity of distilled water for the gel composition, respectively. Solutions of metal ace-

Table 1
Final molar compositions of the reaction mixtures and the synthesis conditions for the preparation of $AlPO_4$-31 and MeAPO-31 products

Products	MeO	Al_2O_3	P_2O_5	Pr_2NH	H_2O	pH		T (d^{-1})[a]	T ($(°C)^{-1}$)
						i[a]	f[a]		
$AlPO_4$-31	–	1.2	1	3	40	7.5	10	2	200
CoAPO-31	0.1	0.95	1	1	50	8.5	9	3	200
MnAPO-31	0.1	0.95	1	1	50	8.5	9	3	200

[a] i: initial pH value; f: final pH value; d: days.

tate and orthophosphoric acid were successively added to the pseudo-boehmite dispersion. Finally, di-*n*-propylamine as the organic template was added dropwise. Using the disperser, the system was thoroughly blended to a homogeneous mixture each time before the addition of the next component. The reaction mixture was seeded with $AlPO_4$-31.

The resulting gels were transferred to 50 ml stainless steel teflon-lined autoclaves and heated under static conditions in an oven. After crystallization was complete, the $AlPO_4$-31 and MeAPO-31 crystals were washed with distilled water three times and dried at 105 °C. Template-free (calcined) samples were prepared by heating the as-synthesized products (calcination process) to 550 °C using a heating rate of 2 °C/min and holding at that temperature, in an air or oxygen flow, for 6 h. The colors of the as-synthesized and calcined products are given in Table 2.

3. Characterization

X-ray powder diffraction (XRPD) patterns of all products were collected on a Siemens D-5000 diffractometer using CuKα radiation at room temperature. The XRPD data were collected in the 2θ range from 5° to 35° in steps of 0.04°, with 1 s per step. Temperature-resolved patterns of selected samples in air were collected on the same diffractometer equipped with an HTK-16 high-temperature chamber. The 2θ range was from 5° to 38°, the step size was 0.026° with 4 s per step. Patterns were collected at selected temperatures between room temperature and 1000 °C. Between the scans the sample was heated at a rate of 10 °C/min.

Table 2
Colors of as-synthesized and calcined materials

Product	As-synthesized	Calcined in an air flow	Calcined in an oxygen flow
$AlPO_4$-31	White	White	White
CoAPO-31	Blue	Blue	Green
MnAPO-31	White	Violet	Violet

The size and the morphology of the crystals were studied with a scanning electron microscope Jeol JXA-840A. Elemental analysis was carried out with an energy dispersion analysis by X-ray analytical system (TRACOR EDX), attached to the scanning electron microscope (Jeol JXA-840A). The C, H and N elemental analysis was performed using a Perkin-Elmer 2400 elemental analyzer. For thermogravimetric analysis (TGA) and differential scanning calorimetry (DSC) a TA 2000 Thermal Analyzer (TA Instruments, Inc.) and an inert atmosphere were used. Measurements were carried out in a flow of He (50 cm^3/min) with a heating rate of 10 °C/min.

Static ^{31}P NMR spectra of CoAPO-31 were obtained on a Varian Unity Inova spectrometer, operating at 242.89 MHz for phosphorus nuclei, according to the spin-echo mapping technique [23,24]. A series of Fourier-transformed echo spectra were recorded using a conventional Hahn-echo sequence, by incrementing the irradiation frequency with a constant step of 34.5 kHz below and above the phosphorus resonance of H_3PO_4. The number of increments was 50. The length of a 90° pulse was 7.25 μs, and the delay before and after the 180° pulse was 20 μs. After Fourier transformation, the height of each spectrum was corrected to take into account effects of transverse relaxation. For this purpose, the ^{31}P T_2 relaxation time was measured at each carrier frequency. After correction, spectra were added according to a

method proposed by Tong [23], and final spin-echo mapping spectra were obtained.

UV–VIS spectra of solid samples were recorded on a UV–VIS spectrophotometer (Lambda 19). Products were suspended in nujol on filter paper and measured in the normal solution cell container [25].

The X-ray absorption spectra at the Co and Mn K-edge were measured at the E4 synchrotron radiation station of HASYLAB, DESY. The station provides a focused beam from an Au-coated mirror and an Si(1 1 1) double crystal monochromator with about 1 eV resolution at the Co K-edge. Harmonics are effectively eliminated by a plane Au-coated mirror and by a slight detuning of the monochromator crystals, keeping the intensity at 60% of the rocking curve with the beam stabilization feedback control. Powder samples were prepared on multiple layers of adhesive tape. Due to the low concentration of transition metal in the samples, a K-edge jump of 0.2 was obtained in the case of Mn and 0.04 for Co. Reference spectra were measured on empty tapes without the sample. Exact energy calibration is established with the simultaneous absorption measurements on the respective (Mn or Co) metal sample.

The acidity of the catalysts was assessed qualitatively using a Nicolet Magna-IR 550 series II spectrometer with pyridine and ammonia as probe molecules. The catalysts were activated and reduced in situ at 400 °C under vacuum (10^{-5} mbar). The detailed experimental procedure was described elsewhere [26,27].

4. Results and discussion

4.1. XRPD, elemental and thermogravimetric characterization

Products of the synthesis procedure were identified from their XRPD patterns. $AlPO_4$-31 crystallized as a single phase, while MeAPO-31 (Me = Co, Mn) crystallized with two competing phases, MeAPO-50 [28] and MeAPO-11 [28]. Syntheses having a higher metal-to-aluminum ratio resulted in a lower ratio of structure type 31 with respect to competing phases. Because of a significant difference in densities between the competing phases and phase 31, the latter was easily separated from undesirable phases by sedimentation. The presence of MeAPO-50 and MeAPO-11 crystals in the synthesized products is understandable: di-*n*-propylamine, which was used as a structure-directing agent, is well known as a template for the synthesis of many $AlPO_4$-*n* molecular sieves with straight channels ($AlPO_4$-11, VPI-5 and CoAPO-50 for example) [7]. Following an extensive study and optimization of the synthesis procedures, we believe that products with the highest possible content of heteroatoms (Co, Mn) in the structure type 31 were obtained.

Scanning electron micrographs (SEM) of all products revealed a needle-like morphology. In the case of MnAPO-31 the needles form cauliflower-like aggregates. The micrographs also confirm the purity of the $AlPO_4$-31, MnAPO-31 and CoAPO-31 samples (Fig. 1). Crystal dimensions range from $1 \times 1 \times 20$ to $8 \times 8 \times 80$ μm^3.

The XRPD patterns of the as-synthesized products (Fig. 2) indicate rhombohedral (CoAPO-31, MnAPO-31) and triclinic symmetries ($AlPO_4$-31). According to the literature [3] the rhombohedral lattices of CoAPO-31 and MnAPO-31 indicate the isomorphous substitution of framework atoms by cobalt and manganese.

During thermal treatment $AlPO_4$-31 (Fig. 3A) is stable even above 1000 °C, while CoAPO-31 (Fig. 3B) and MnAPO-31 (Fig. 3C) are stable up to 590 and 560 °C, respectively. Above these temperatures the structures collapse into an $AlPO_4$-tridymite dense phase and an amorphous phase. The powder patterns of as-synthesized $AlPO_4$-31, under thermal treatment in air, shows that at 210 °C a transformation from triclinic to rhombohedral symmetry occurs (Fig. 3A).

On the basis of elemental and thermogravimetric analyses of the $AlPO_4$-31 and MeAPO-31 (Me = Co, Mn) crystals, the general formulae $(Me_xAl_yP_z)O_2$ were calculated (Table 3). The value of $x + y \approx z \approx 0.5$ in the general formulae indicates that aluminum in the $AlPO_4$-31 framework was isomorphously substituted by metals [29]. For cobalt and manganese, a 5% isomorphous aluminum substitution is suggested. One can also notice that the triclinic $AlPO_4$-31 material contains twice

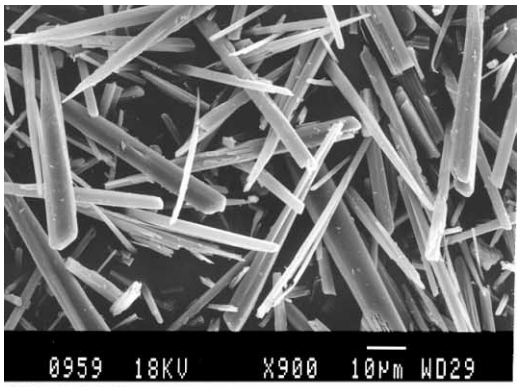

Fig. 1. SEM photographs of (A) $AlPO_4$-31, (B) CoAPO-31 and (C) MnAPO-31.

as much template as the rhombohedral CoAPO-31 and MnAPO-31 materials (Table 3). Furthermore, thermogravimetric and elemental analyses show that, in as-synthesized $AlPO_4$-31, the transformation from triclinic to rhombohedral symmetry occurs when just one half of the template molecules are expelled from the pores of the sample. This indicates that the interaction between the metal incorporated into the framework and the template may be responsible for the symmetry changes for the as-synthesized MeAPO-31 product, and this phenomenon requires a further study.

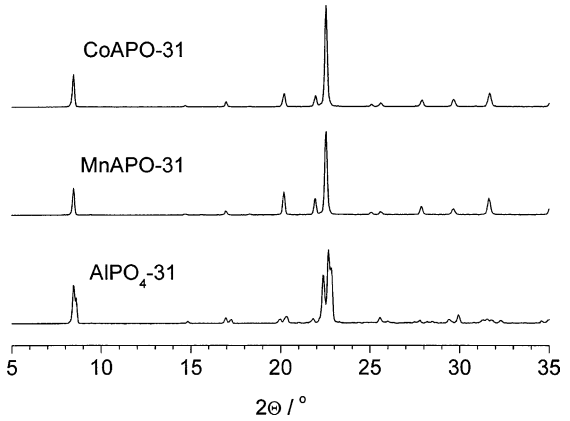

Fig. 2. XRPD patterns of as-synthesized $AlPO_4$-31, CoAPO-31 and MnAPO-31.

The results of the TGA reveal some similarities betweeen CoAPO-31 and MnAPO-31 (Fig. 4). The TGA/DTA profiles of as-synthesized $AlPO_4$-31 in an inert atmosphere show that the desorption of water takes place up to 180 °C and that the decomposition of di-*n*-propylamine occurs between 180 and 500 °C. The origin of the weight loss (i.e., whether it is due to the desorption of water or due to the removal of the template) was determined with the aid of elemental analysis for C, H and N of the as-synthesized sample. The TGA/DTA profiles of as-synthesized MnAPO-31 and CoAPO-31 show that desorption of water ends at about 140 °C, and the decomposition of di-*n*-propylamine occurs between 140 and 550 °C. For MnAPO-31 and CoAPO-31 the decomposition of the template occurs in two steps. The second step is probably due to a location of the template molecules close to the Brønsted and Lewis acid sites, which are expected to be present in MeAPOs [30]. The DSC profiles (Fig. 4) for all samples show endothermic peaks, which is consistent with a desorption of water and decomposition of the template in the inert atmosphere.

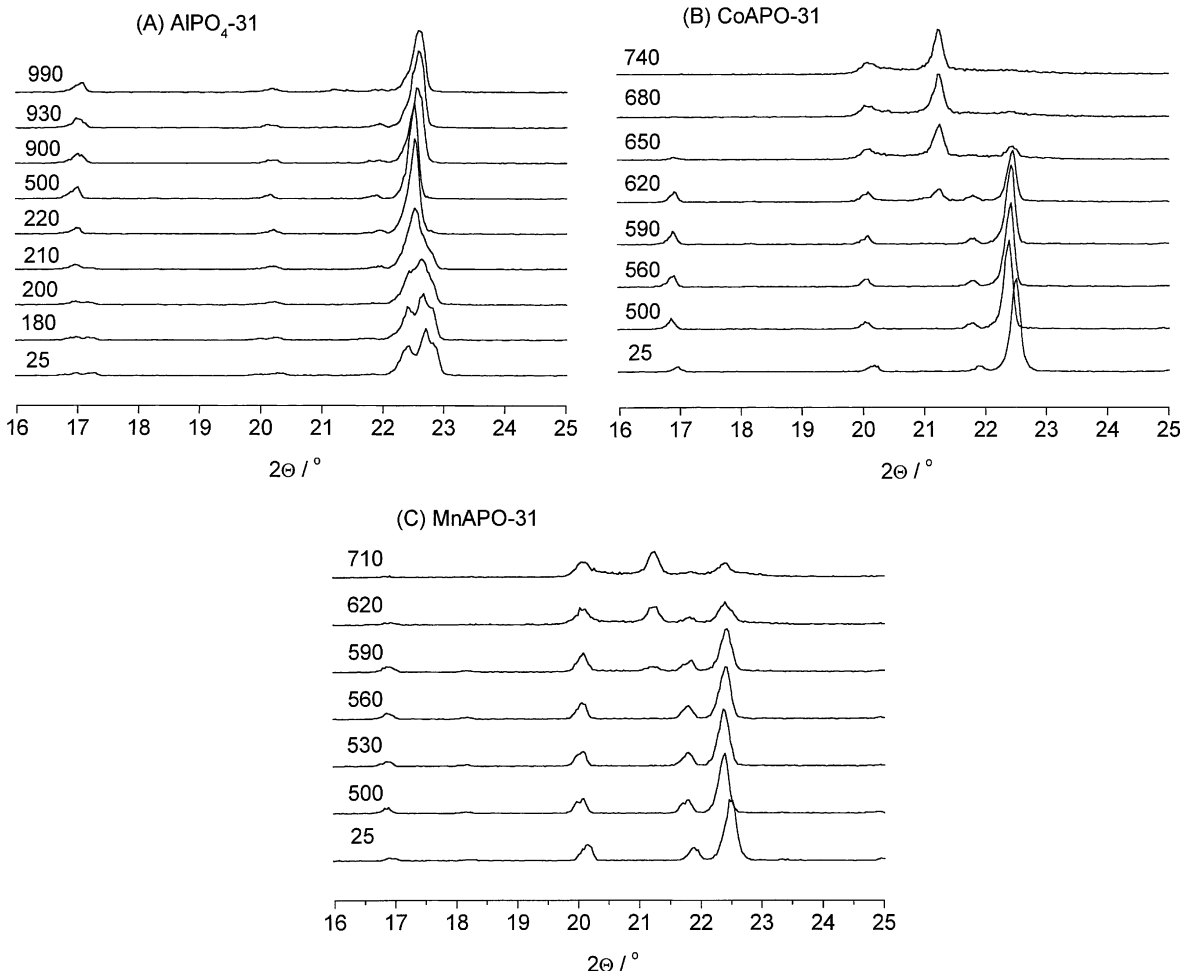

Fig. 3. XRPD patterns of $AlPO_4$-31 (A), CoAPO-31 (B) and MnAPO-31 (C), measured during thermal treatment of the samples in air.

Table 3
Chemical compositions of the products (uncertainty of the (x, y, z) data is ±0.005)

Sample	TO_2 formula $(Me_xAl_yP_z)O_2$			DIP/TO_2	DIP/H_2O
	x	y	z		
$AlPO_4$-31		0.499	0.501	0.047	0.018
CoAPO-31	0.023	0.474	0.503	0.025	0.029
MnAPO-31	0.026	0.473	0.501	0.025	0.014

DIP: di-*n*-propylamine.

4.2. NMR study of isomorphous aluminum substitution by cobalt

Direct evidence for the substitution of aluminum by cobalt can be obtained from NMR spectroscopy. It was demonstrated on a number of CoAPO-*n* materials that, using the so-called spin-echo mapping technique, one can efficiently record broad-line static ^{31}P spectra and prove or disprove cobalt incorporation [24].

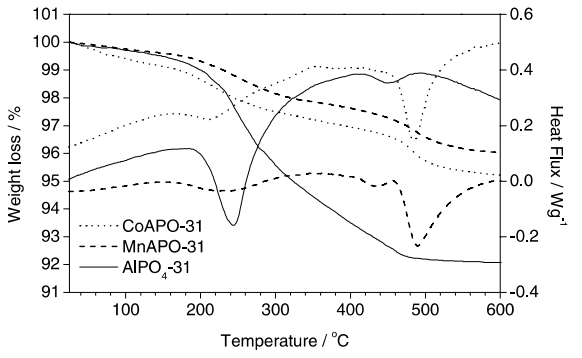

Fig. 4. TG/DSC profiles of $AlPO_4$-31, CoAPO-31 and MnAPO-31.

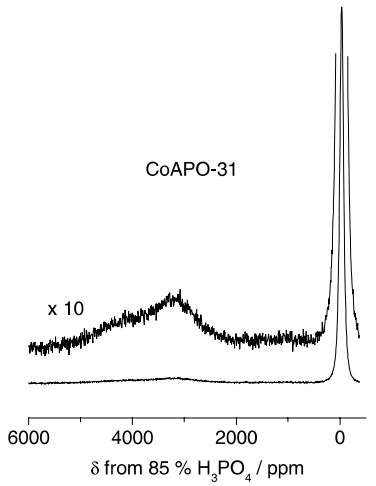

Fig. 5. Static ^{31}P NMR spectrum of as-synthesized CoAPO-31 obtained by the spin-echo mapping technique.

A static ^{31}P spectrum of as-synthesized CoAPO-31 is presented in Fig. 5. In addition to a strong peak at about 0 ppm, there is a low and broad feature extending from about 2000 to about 5500 ppm. According to the literature [24] this is approximately the range of P(1Co, 3Al) and P(2Co, 2Al) units. Because cobalt within the cavities does not shift the phosphorus resonance, the broad shifted peak confirms cobalt incorporation into aluminum framework sites.

The relative intensities of the sharp and broad peak are 0.81 ± 0.02 and 0.19 ± 0.02, respectively. From these measured data one can deduce the fraction of cobalt incorporated into the framework, if the following is taken into account: all phosphorus atoms are crystallographically equivalent; the incorporation of cobalt is random; no clusters of cobalt are formed within the sample. For random incorporation, the probability that phosphorus is surrounded by nCo atoms and (4-n)Al atoms is given by:

$$P(n\mathrm{Co}) = \frac{4!}{(4-n)!n!} p^n (1-p)^{(4-n)} \quad (1)$$

Here p is the probability to find cobalt on an aluminum position ($p = n_{\mathrm{Co}}/(n_{\mathrm{Co}} + n_{\mathrm{Al}})$). Taking into account the measured value $P(0\mathrm{Co}) = 0.19$ we obtain the probability (p) for the incorporation of Co equal to 0.051 ± 0.006. This is in a good agreement with the result of elemental analysis, which gives ($p = n_{\mathrm{Co}}/(n_{\mathrm{Co}} + n_{\mathrm{Al}})$) equal to 0.046 ± 0.005.

4.3. UV–VIS absorption spectra—co-ordination geometry of cobalt and manganese

The co-ordination geometry of incorporated manganese and cobalt is indicated by the UV–VIS absorption spectra. Figs. 6 and 7 show, respectively, absorption spectra of as-synthesized and calcined CoAPO-31 and MnAPO-31. The absorption bands of all samples at 240 nm are related

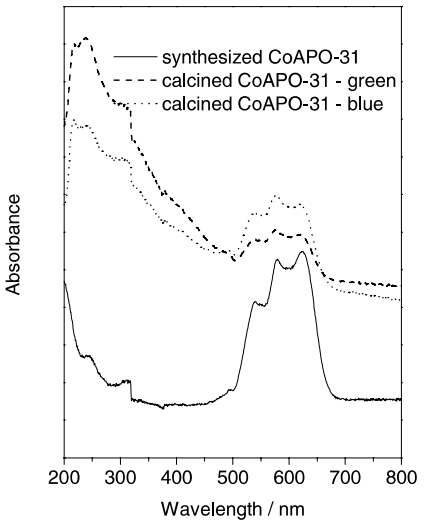

Fig. 6. UV–VIS spectra of as-synthesized and calcined CoAPO-31.

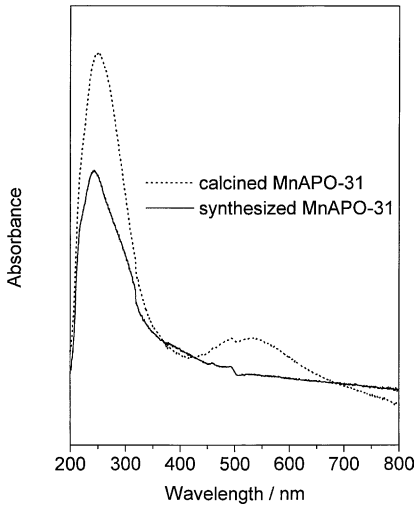

Fig. 7. UV–VIS spectra of as-synthesized and calcined MnAPO-31.

to the charge transfer processes between framework aluminum and oxygen atoms of the aluminophosphate and water molecules [31].

The UV–VIS spectra of as-synthesized CoAPO-31 and both the (blue and green) calcined CoAPO-31 samples (Fig. 6) show three maxima in the region between 450 and 700 nm corresponding to tetrahedrally co-ordinated Co(II) species [32–34]. Calcined blue and green CoAPO-31 also show a broad absorption from 315 to 400 nm, which can be attributed to a ligand–metal charge transfer from a framework electron to Co(III) [33,34]. The electronic spectra indicate that tetrahedrally coordinated Co(II) and Co(III) cations are present in both the blue and green calcined samples of CoAPO-31. The color changes observed during the calcination process are usually associated with changes in the electronic environment (e.g., ligand field effects) or with changes of the oxidation state of the incorporated metal. In our case, we expect that changes in the electronic environment are taking place, and that they are induced by the calcination atmosphere. Calcination in oxygen flow caused the color to change from blue to green while calcination in air flow did not. The reason for this is not clear.

Fig. 7 shows absorption spectra of the as-synthesized and calcined MnAPO-31 products. The spectrum of the white as-synthesized MnAPO-31 is not informative at wavelengths in the visible region. The position of the absorption maximum in the spectrum of the violet calcined MnAPO-31 is similar to that of Mn(III) complexes, octahedrally coordinated by oxygen-donor ligands [34,35]. The electronic spectra indicate that both Mn(II) and Mn(III) cations are present in the calcined MnAPO-31.

4.4. EXAFS and XANES studies—local symmetry of cobalt and manganese

The normalized Co and Mn XANES spectra of the as-synthesized and calcined samples (Figs. 8 and 9) are extracted by a standard procedure [36]. The zero energy is taken at the first inflection point in the cobalt and manganese metal spectrum, respectively, that is at the 1s ionization threshold in the cobalt and manganese metal.

The shape of the K-edge and the pre-edge resonances are characteristic for the local symmetry of the investigated atom and can be used as fingerprints in the identification of its local structure [36,37]. Tetrahedrally coordinated atoms exhibit a single pre-edge peak, which can be assigned to a 1s $\rightarrow$ 3d transition. This transition is prominent only

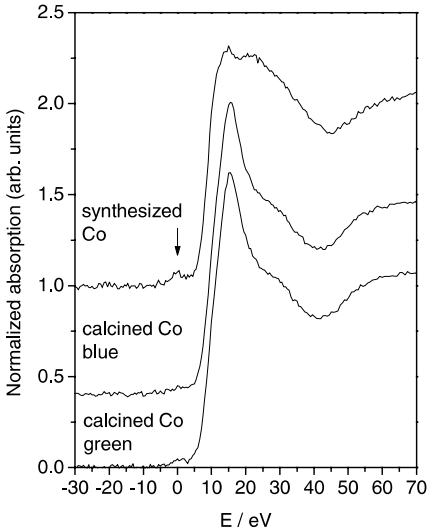

Fig. 8. Normalized Co K-edge profiles of CoAPO-31 samples, displaced vertically for clarity. The energy scale is relative to the Co K-edge in the metal (7709.0 eV).

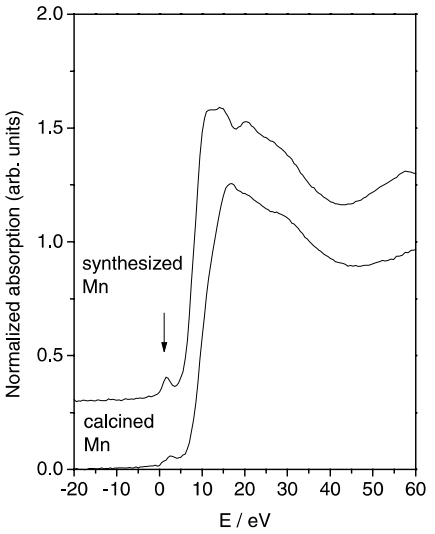

Fig. 9. Normalized Mn K-edge profiles of MnAPO-31 samples, displaced vertically for clarity. The energy scale is relative to Mn K-edge in the metal (6539.0 eV).

in atoms located at the sites without a center of inversion, and it is forbidden for atoms occupying sites with inversion symmetry. Co and Mn XANES spectra of as-synthesized products (CoAPO-31 and MnAPO-31) exhibit the characteristic tetrahedral pre-edge resonance, demonstrating that metal cations are incorporated into the tetrahedral sites [22,38–40]. In XANES spectra of the calcined samples, the pre-edge peak is strongly diminished or completely absent, which indicates that in the process of calcination the tetrahedral environment of the metal is distorted.

Changes in the valence state of the incorporated metal cation during calcination can be deduced from the energy shift of the absorption edge [36,37]. A linear relation between the edge shift and the valence state was established for the atoms having the same type of ligand [36,37]. For cobalt atoms shifts of 1.5–3 eV per valence are reported [22], while for manganese atoms a shift of 3.5 eV per valence is found [39]. In the case of CoAPO-31 both calcined samples exhibit the same Co K-edge energy shift of 1.0 ± 0.3 eV compared to the as-synthesized material, indicating a partial oxidation of Co(II) during the calcination. Approximately the same amount of Co(III) is present after calcination procedures in different atmospheres—in oxygen flow and in air flow. Our measurements show that the Mn K-edge in the calcined MnAPO-31 sample is shifted by 1.5 ± 0.2 eV compared to the edge position in the as-synthesized (uncalcined) sample. This shift suggests an increase of 0.4 ± 0.1 in the average manganese oxidation number, which suggests that in the process of calcination almost one half of the framework manganese(II) is oxidized to manganese(III).

The EXAFS spectra were analyzed using the UWXAFS and FEFF6 code [41,42] in the k-range 3–11 X^{-1}, using a k weighted Hanning window. Fourier transforms of k weighted Co and Mn EXAFS spectra are shown in Figs. 10 and 11, respectively. Due to the relatively low signal to noise ratio, only the parameters of the first coordination shell can be reliably determined.

In modeling Co EXAFS spectra, the fit of the first coordination shell in the R range 0.9–2.1 Å shows that in the as-synthesized sample cobalt atoms are coordinated to four oxygen atoms eachat 1.96 Å, in accordance with the presumed insertion of cobalt cations into the tetrahedral sites of the CoAPO-31 framework. Four oxygen neighbors are found also in the calcined samples,

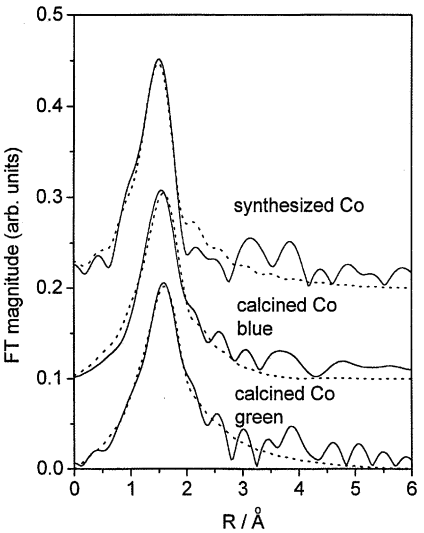

Fig. 10. Fourier transforms of k weighted EXAFS spectra of as-synthesized and calcined CoAPO-31 samples. Experiment (—); fit (···).

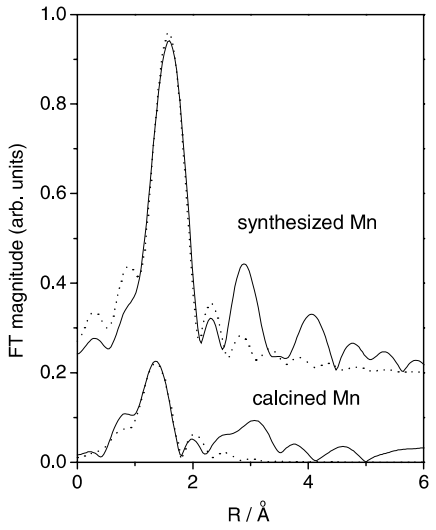

Fig. 11. Fourier transforms of k weighted EXAFS spectra of as-synthesized and calcined MnAPO-31 samples. Experiment (—); fit (···).

but at a larger distance (2.07 Å). Additionally, an increase in the Debye-Waller factor is observed (Table 4), indicating larger static disorder in the first coordination shell of cobalt in the calcined samples.

A fit of the Mn EXAFS spectra in the R range 1.0–2.2 Å shows that manganese has four oxygen neighbors at 2.02 Å in the as-synthesized sample, indicating the incorporation of manganese(II) into tetrahedral framework sites. After calcination, the local environment of manganese atoms is significantly changed. A decrease in the number of oxygen atoms in the first coordination shell can be seen from the height of the first peak in the FT spectra (Fig. 11). A quantitative analysis shows that manganese atoms are on the average coordinated to three oxygen atoms: one at 1.87 Å and two at 2.08 Å.

A large Debye-Waller factor is found for the more distant oxygen atoms indicating larger statistical disorder at that distance. Best-fit parameters are listed in Table 4. Relatively large uncertainties of N and σ^2 are a consequence of strong correlations between the two parameters in the fit.

The XANES and EXAFS results confirm the incorporation of Co and Mn into tetrahedral framework sites in the synthesized samples. In the case of Co, a partial oxidation in the process of calcination is indicated by the XANES spectra, but we have not found any short Co–O distances characteristic for Co(III) cations. However, larger statistical disorder is found in the first Co coordination shell in the calcined sample, so a smaller amount of Co(III) with shorter Co–O distances may be present, but cannot be discerned from the EXAFS spectrum due to the relatively low signal to noise ratio.

In the process of calcination part of the Mn(II) is oxidized to Mn(III), which can be seen from the XANES spectra. The presence of Mn(III) is also confirmed by EXAFS, where short Mn–O distances, characteristic of trivalent Mn cations, are observed. In calcined MnAPO-31, manganese atoms are coordinated on average to three oxygen

Table 4
Best fit parameters of the first coordination shell of Co and Mn cations in the crystal structure of CoAPO-31 and MnAPO-31 samples: number of neighbors N at the distance R, and Debye-Waller factor σ^2 (uncertainty of the last digit is given in parentheses)

Sample		N	R (Å^{-1})	σ^2 ((Å^2)$^{-1}$)
CoAPO-31	Co neighbor			
Synthesized	O	3.8(4)	1.96(1)	0.003(1)
Calcined blue (air)	O	3.8(8)	2.06(1)	0.006(3)
Calcined green (oxygen)	O	4.4(5)	2.07(1)	0.009(1)
MnAPO-31	Mn neighbor			
Synthesized	O	3.7(9)	2.02(1)	0.004(2)
Calcined	O	1.1(6)	1.87(3)	0.003(2)
	O	1.5(3)	2.08(7)	0.015(9)

atoms. This could be explained by the formation of a defect center by creation of a framework oxygen vacancy as observed previously in ZnAPO-34 [43]. The defect center with a framework oxygen vacancy was previously described for CoAPO-44 using ab initio quantum chemical techniques applied to the investigation of structural and bonding properties of cobalt-substituted aluminophosphates [21].

4.5. In situ IR measurements of pyridine and ammonia adsorption/desorption—acidity of CoAPO-31 and MnAPO-31

Pyridine and ammonia are probe molecules used routinely for the characterization of acid sites in solids by infrared spectroscopy [44]. Pyridine is usually preferred because spectral interpretation is simpler than in the case of ammonia [45]. In this study we used both probe molecules for comparison with known reference solids. Ammonia was sorbed at ambient temperature, but pyridine was sorbed at 150 °C to limit diffusion problems.

The electroneutrality of the $AlPO_4$-31 framework should preclude the development of Brønsted acidity [46]. Indeed, the difference FTIR spectra (subtraction of parent spectrum from the spectrum of sample plus sorbate) using either of the probe molecules show only weak signals, for Brønsted or Lewis acid sites, and these signals were readily removed on heating. In this work pyridine was adsorbed at 150 °C, to avoid diffusion limitations, and the sample was heated under vacuum at the same temperature to remove physisorbed species. Ammonia was adsorbed at room temperature [46,47]. In the case of pyridine sorption, bands at 1545 and 1450 cm^{-1} are indicative [46,47] of Brønsted and Lewis sites, respectively (Fig. 12A). For adsorbed ammonia [46] the corresponding bands are at 1453 and 1618 cm^{-1} (Fig. 13A).

The difference spectrum of $AlPO_4$-31 in the OH region (Fig. 14A), upon ammonia adsorption, shows a band at 3677 cm^{-1}, which can be assigned to either a P–OH or an Al–OH group [26,27]. On sorption of ammonia this appears as a negative peak for the parent material. Other bands evident at 3385, 3293 and 3197 cm^{-1} are due to N–H stretching, associated with weakly bonded ammonia, which can be completely desorbed from the

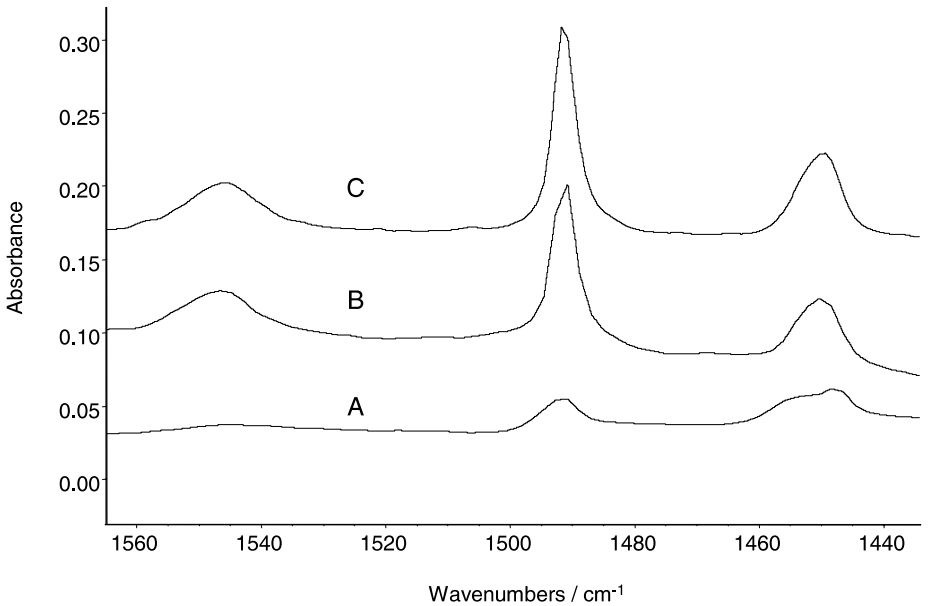

Fig. 12. FTIR difference spectra after pyridine adsorption at 150 °C on (A) $AlPO_4$-31, (B) CoAPO-31 and (C) MnAPO-31.

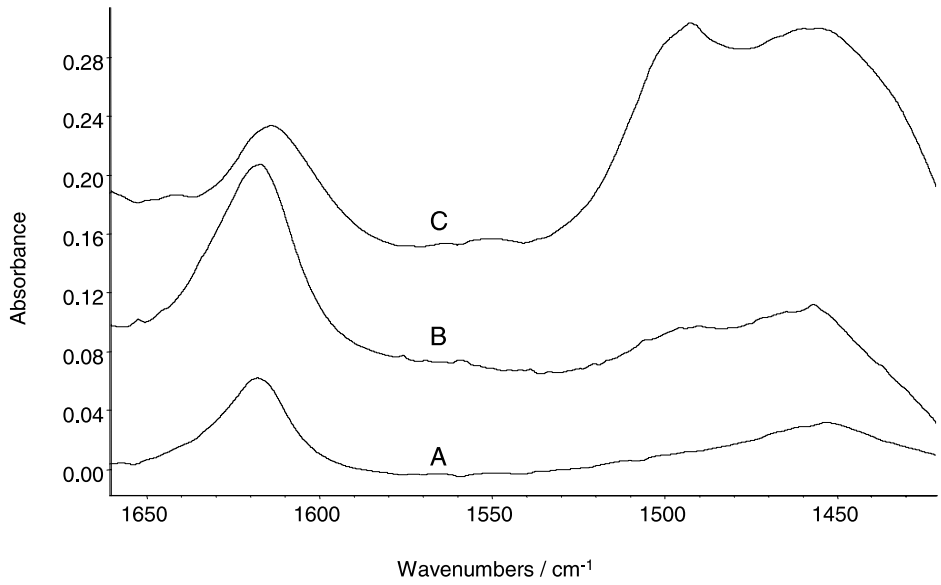

Fig. 13. FTIR difference spectra after ammonia adsorption at ambient temperature on (A) $AlPO_4$-31, (B) CoAPO-31 and (C) MnAPO-31.

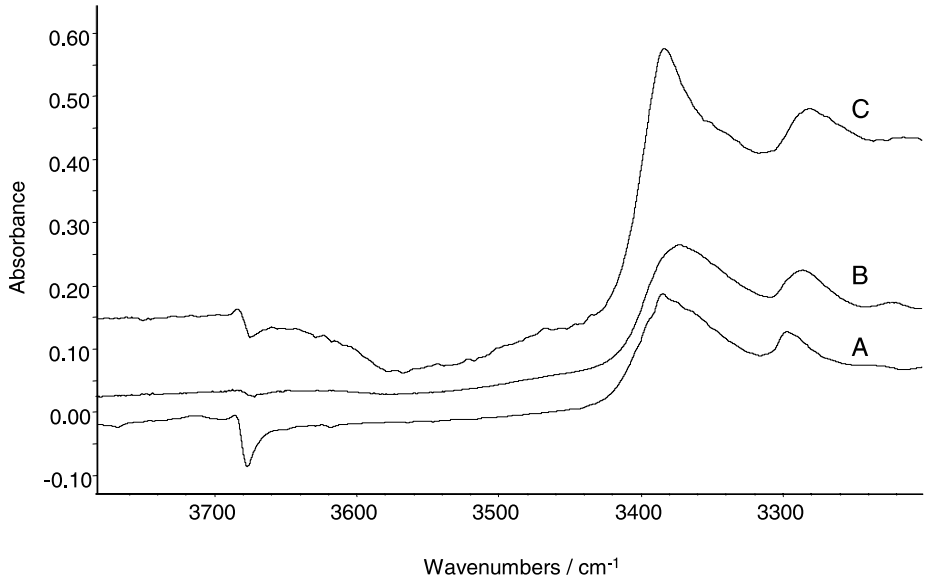

Fig. 14. OH-region of FTIR difference spectra after ammonia adsorption at ambient temperature on (A) $AlPO_4$-31, (B) CoAPO-31 and (C) MnAPO-31.

sample at 100 °C. Therefore, we may conclude that the $AlPO_4$-31 sample does not contain acid sites in appreciable amounts.

Al(III) substitution by Me(II) (Mn and Co) in the framework of $AlPO_4$-31 clearly generates both Brønsted and Lewis acid sites. This is evident from

the adsorption of pyridine and ammonia on all the samples prepared in this study (Figs. 12 and 13). Bands due to Py–H^+ at 1545 cm^{-1} (Brønsted sites) and at 1450 cm^{-1} (Lewis acid sites) are observed in all MeAPO-31 materials (Fig. 12). However, the intensities of the bands due to pyridinium ions on the MnAPO-31 sample are much higher and are removed at higher desorption temperature (400 °C) in comparison with the other samples. The difference spectrum of MnAPO-31 after ammonia adsorption (Fig. 14C) exhibits a negative peak at 3678 cm^{-1}, assigned to non-acidic hydroxyls (P–OH) [47,48], a broad negative band around 3560 cm^{-1} assigned to bridged MnP-OH groups, and intense positive peaks at 3400 and 3300 cm^{-1} assigned to NH_4^+-ions formed by interaction of ammonia with acidic hydroxyls. Bands associated with acidic hydroxyls, which give rise to NH_4^+-ions are less pronounced in the case of CoAPO-31. Similar observations have been reported for other substituted MeAPO series [47,48].

The strength of acid sites generated in the samples studied here is assessed in situ via thermodesorption of adsorbed ammonia and pyridine. In order to remove all the sorbed ammonia from acid sites generated in MnAPO-31 a temperature of 400 °C is needed. On the other hand, for the CoAPO-31 sample, a desorption temperature of around 300 °C is sufficient. In the case of the $AlPO_4$-31 sample, the adsorbed pyridine is completely removed below 250 °C and the ammonia at 100 °C. Based on the above observations the strength of acid sites (Brønsted and Lewis) generated in the catalysts prepared in this work shows the following trend: MnAPO-31 > CoAPO-31 > $AlPO_4$-31.

5. Conclusions

The isomorphous substitution of framework aluminum in $AlPO_4$-31 by cobalt and manganese was confirmed.

It was also found that the relation between the metal incorporated into the framework sites and the template might be responsible for the symmetry changes for the as-synthesized MeAPO-31 as compared to $AlPO_4$-31. The symmetry transformation of aluminophosphate molecular sieve $AlPO_4$-31 and the interaction of its framework with di-*n*-propylamine template molecules were, therefore, further studied by variable temperature XRPD and multinuclear MAS, CPMAS and MQMAS NMR measurements [49].

Brønsted and Lewis acid sites and also redox active centers were detected and characterized in MeAPO-31. In proposed further work the potential of MnAPO-31 and CoAPO-31 as catalysts in oxidation reactions will be tested.

Acknowledgements

The authors acknowledge the financial support of the Ministry of Education, Science and Sport through the research project no. Z2-3457-0104.

References

[1] J.M. Bennett, R.M. Kirchner, Zeolites 12 (1992) 338.
[2] W.H. Baur, W. Joswig, D. Kassner, J. Kornatowski, Acta Cryst. B 50 (1994) 290.
[3] G. Finger, J. Kornatowski, K. Jancke, R. Matschat, W.H. Baur, Micropor. Mesopor. Mater. 33 (1999) 127.
[4] L. Zubowa, E. Alsdorf, R. Fricke, F. Neissendorfer, J. Richter-Mendau, E. Schreier, D. Zeigan, B. Zibrowius, J. Chem. Soc., Faraday Trans. 86 (1990) 2307.
[5] B. Zibrowius, E. Löffler, M. Hunger, Zeolites 12 (1992) 167.
[6] A.M. Prakash, S.V.V. Chilukuri, R.P. Bagwe, S. Ashtekar, D. Chakrabarty, Micropor. Mater. 6 (1966) 89.
[7] A.K. Sinha, S. Sainkar, S. Sivasanker, Micropor. Mesopor. Mater. 31 (1999) 321.
[8] H.L. Zubowa, M. Richter, U. Roost, B. Parlitz, R. Fricke, Catal. Lett. 19 (1993) 67.
[9] H.L. Zubowa, G. Lischke, B. Parlitz, E. Schreier, R. Eckelt, G. Schulz, R. Fricke, Appl. Catal. A: General 110 (1994) 27.
[10] M. Richter, R. Eckelt, H.L. Zubowa, React. Kinet. Catal. Lett. 53 (1994) 309.
[11] C.M. López, F.J. Machado, J. Goldwasser, B. Méndez, K. Rodríguez, M.M. Ramírez-Agudelo, Zeolites 19 (1997) 133.
[12] P. Mériaudeau, V.A. Tuan, V.T. Nghiem, S.Y. Lai, L.N. Hung, C. Naccache, J. Catal. 169 (1997) 55.
[13] A.M. Prakash, L. Kevan, M. Hassan Zahedi-Niaki, S. Kaliaguine, J. Phys. Chem. B 103 (1999) 831.
[14] O.V. Kikhtyanin, R.F. Vogel, C.L. Kibby, T.V. Harris, K.G. Ione, D.J. O'Rear, in: M.M.J. Treacy, B.K. Marcus, M.E. Bisher, J.B. Higgins (Eds.), Proceedings of the 12th International Zeolite Conference, Vol. 3, Materials Research Society, Warrendale, 1999, p. 1743.

[15] M. Hassan Zahedi-Niaki, M.P. Kapoor, S. Kaliaguine, in: M.M.J. Treacy, B.K. Marcus, M.E. Bisher, J.B. Higgins (Eds.), Proceedings of the 12th International Zeolite Conference, Vol. 3, Materials Research Society, Warrendale, 1999, p. 1221.
[16] N. Venkatathri, S.G. Hegde, S. Sivasanker, J. Chem. Soc., Chem. Commun. (1995) 151.
[17] V. Umamaheswari, C. Kannan, B. Arabindoo, M. Palanichamy, V. Murugesan, Proc. Indian Acad. Sci. (Chem. Sci.) 112 (2000) 439.
[18] M. Dugal, G. Sankar, R. Raja, J.M. Thomas, Angew. Chem. Int. Ed. 39 (2000) 2310.
[19] J.M. Thomas, R. Raja, G. Sankar, R.G. Bell, Nature 398 (1999) 227.
[20] M. Hartmann, L. Kevan, Chem. Rev. 99 (1999) 635.
[21] F. Corà, C.R.A. Catlow, A. D'Ercole, J. Mol. Catal. A: Chem. 166 (2001) 87.
[22] P.A. Barrett, G. Sankar, C.R.A. Catlow, J.M. Thomas, J. Phys. Chem. 100 (1996) 8977.
[23] Y.Y.J. Tong, Magn. Reson. A 119 (1996) 22.
[24] L. Canesson, Y. Boudeville, A. Tuel, J. Am. Chem. Soc. 119 (1997) 10754.
[25] R.J. Butcher, G. Diven, G. Erickson, J. Jasinski, G.M. Mockler, R.Y. Pozdniakov, E. Sinn, Inorg. Chim. Acta 239 (1995) 107.
[26] V.L. Zholobenko, M.A. Makarova, J. Dwyer, J. Phys. Chem. 93 (1993) 5962.
[27] M.A. Makarova, V.L. Zholobenko, A. Garforth, J. Dwyer, G.J. Earl, D. Rawlence, in: J. Weitkamp, H.G. Karge, H. Pfeifer, W. Hölderich (Eds.), Zeolites and Related Microporous Materials: State of the Art 1994, Studies in Surface Science and Catalysis, Part A, Vol. 84, Elsevier, Amsterdam, 1994, p. 365.
[28] M.M.J. Treacy, J.B. Higgins, in: Collection of Simulated XRD Powder Patterns for Zeolites, Elsevier, New York, 2001, pp. 24–25, pp. 46-47.
[29] E.M. Flanigen, R.L. Patton, S.T. Wilson, in: P.J. Grobet, W.J. Mortier, E.F. Vansant, G. Schulz-Ekloff (Eds.), Innovation in Zeolite Materials Science, Studies in Surface Science and Catalysis, Vol. 37, Elsevier, Amsterdam, 1988, p. 13.
[30] S. Coluccica, L. Marchese, G. Martra, Micropor. Mesopor. Mater. 30 (1999) 43.
[31] M.A. Zanjanchi, M.K. Rashidi, Spectrochim. Acta, Part A 55 (1999) 947.
[32] A.A. Verbeckmoes, M.G. Uytterhoeven, R.A. Schoonheydt, Zeolites 19 (1997) 180.
[33] L. Canesson, A. Tuel, Zeolites 18 (1997) 260.
[34] N. Rajić, I. Arčon, V. Kaučič, A. Kodre, Croatica Chem. Acta 72 (1999) 645.
[35] A.B.P. Lever, in: Inorganic Electronic Spectroscopy, Elsevier, Amsterdam, 1984, p. 533.
[36] J. Wong, F.W. Lytle, R.P. Messmer, D.H. Maylotte, Phys. Rev. B 30 (1984) 5596.
[37] I. Arčon, B. Mirtić, A. Kodre, J. Am. Ceram. Soc. 81 (1998) 222.
[38] J. Chen, G. Sankar, J.M. Thomas, R. Xu, G. Neville-Greaves, D. Waller, Chem. Mater. 4 (1992) 1373.
[39] T. Ressler, S.L. Brock, J. Wong, S.L. Suib, J. Synchrot. Rad. 6 (1999) 728.
[40] I. Arčon, N. Rajić, A. Kodre, J. Synchrot. Rad. 6 (1999) 460.
[41] E.A. Stern, M. Newville, B. Ravel, Y. Yacoby, D. Haskel, Physica B 208/209 (1995) 117.
[42] J.J. Rehr, R.C. Albers, S.I. Zabinsky, Phys. Rev. Lett. 69 (1992) 3397.
[43] N. Novak Tušar, V. Kaučič, S. Geremia, G. Vlaic, Zeolites 15 (1995) 708.
[44] G. Müller, E. Bodis, J. Kornatowski, J.A. Lercher, Phys. Chem. Chem. Phys. 1 (1999) 571.
[45] A. Zecchina, L. Marchese, S. Bordiga, C. Paze, E. Gianotti, J. Phys. Chem. B 101 (1997) 10128.
[46] V. Zholobenko, A. Garforth, L. Clark, J. Dwyer, in: L. Bonneviot, S. Kaliaguine (Eds.), Zeolites: A Refined Tool for Designing Catalytic Sites, Studies in Surface Science and Catalysis, Vol. 97, Elsevier, Amsterdam, 1995, p. 359.
[47] M. Höchtl, A. Jentys, H. Vinek, Micropor. Mesopor. Mater. 31 (1999) 271.
[48] B. Craushaar-Czarnetzki, W.G.M. Hoogervorst, R.R. Andrea, C.A. Emies, W.H.Y. Stork, J. Chem. Soc., Faraday Trans. 87 (1991) 891.
[49] G. Mali, A. Meden, A. Ristić, N. Novak Tušar, V. Kaučič, J. Phys. Chem. 106 (2002) 63.